

Resistance of multilayers with long length scale interfacial roughness

Jason Alicea*[†] and Selman Hershfield[‡]

*Department of Physics and National High Magnetic Field Laboratory,
University of Florida, Gainesville, FL 32611-8440*

(Dated: October 28, 2018)

The resistance of multilayers with interface roughness on a length scale which is large compared to the atomic spacing is computed in several cases via the Boltzmann equation. This type of roughness is common in magnetic multilayers. When the electronic mean free paths are small compared to the layer thicknesses, the current flow is non-uniform, and the resistance decreases in the Current-Perpendicular-to-Plane (CPP) configuration and increases in the Current-In-Plane (CIP) configuration. For mean free paths much longer than the layer thicknesses, the current flow is uniform, and the resistance increases in both the CPP and CIP configurations due to enhanced surface scattering. In both the CPP and CIP geometries, the giant magnetoresistance can be either enhanced or reduced by the presence of long length scale interface roughness depending on the parameters. Finally, the changes in the CPP and CIP resistivities due to increasing interface roughness are estimated using experimentally determined parameters.

PACS numbers: 75.70.Pa, 73.40.-c

I. INTRODUCTION

The study of metallic multilayers has been a very active area of research in recent years. Of particular interest are alternating layers of ferromagnetic and paramagnetic metals called magnetic multilayers. A relatively small magnetic field aligns the magnetic moments in the different ferromagnetic layers, leading to a large magnetoresistance, which is called the giant magnetoresistance (GMR).^{1,2} The GMR has technological applications in magnetic read heads, magnetic sensors, and magnetic memory devices. Consequently, it has been studied extensively, including such effects as bulk and interface scattering, magnetic and non-magnetic scattering, Fermi wave vector mismatch and magnetic coupling between the layers.^{3,4,5,6}

One aspect of metallic multilayers which has been less studied theoretically is the effect of long length scale fluctuations of the layer thicknesses and heights. In an ideal multilayer the interfaces between the layers are perfect planes. The thickness of each layer and the height of each layer above the substrate would be constant. Obviously, this is not the case in any real system. In addition to interdiffusion and other atomic scale disorder at the interfaces, the actual thicknesses and/or heights of the layers can vary on a length scale which is large on the atomic scale. Indeed, these long length scale fluctuations seem to be the rule rather than the exception.

Since the Fermi wave vectors for these metals are of order the atomic spacing, interdiffusion and atomic scale disorder are strong sources of scattering. Fluctuations on a length scale of 10 or more atomic spacings should not appreciably effect the surface scattering. Nonetheless,

long length scale disorder can be important. It has been demonstrated both experimentally⁷ and theoretically⁸ that nonplanar interfaces can create new kinds of magnetic coupling between the layers. This tends to reduce the GMR because the fraction of a sample that is antiferromagnetically aligned at zero applied field is reduced. Consequently, many of the experiments that study the role of interfacial roughness rescale the magnetoresistance by the fraction of the sample which is antiferromagnetically coupled. This fraction can be determined experimentally from magnetization measurements.

There are two common geometries used in studying the giant magnetoresistance. The current flows parallel to the layers in the Current-In-Plane (CIP) geometry and normal to the layers in the Current-Perpendicular-to-Plane (CPP) geometry. The CIP geometry has been more widely studied than the CPP geometry because measurements in the CIP configuration are easier to achieve experimentally. Simultaneous measurements of the CIP magnetoresistance and roughness using low angle X-ray scattering have been made on samples with roughness that has been systematically varied by changing growth parameters and annealing. One set of experiments on Fe/Cr multilayers finds that the change in the resistivity between low and high field, $\Delta\rho$, rescaled by the antiferromagnetic fraction, AFF , increases with roughness.^{9,10,11} Schad *et al.* also simultaneously measured the surface roughness and the magnetoresistance of Fe/Cr multilayers.^{12,13,14} In one set of experiments they find that $\Delta\rho/AFF$ decreases with the increasing fluctuations in the layer heights while the saturation resistivity decreases.^{12,13} In another set of experiments on Fe/Cr multilayers which are dominated by surface scattering they find that the CIP magnetoresistance increases with interface fluctuations, which were determined by the ratio of the vertical roughness amplitude to the lateral correlation length.¹⁴

The effect of long length scale roughness on the CIP

*Present address: Department of Physics, University of California, Santa Barbara, California 93117

magnetoresistance has been studied theoretically by Barnas and Bruynseraede¹⁵ and by Levy *et al.*¹⁶ Barnas and Bruynseraede studied the scattering between quantum states in different layers allowing for uncorrelated variations in the layer thicknesses. They find that the magnetoresistance can either increase or decrease with roughness depending on the parameters in the problem. Indeed there are even cases where the magnetoresistance decreases and then increases with roughness. Levy *et al.* studied the magnetoresistance of multilayers deposited on grooved substrates,^{17,18} which produce roughness which is correlated between the layers. Using a general linear response approach they find that the roughness mixes the CIP and CPP geometries, leading to what is called the CAP or Current-at-an-Angle-to-Plane configuration. Since the CIP magnetoresistance is typically smaller than the CPP magnetoresistance, this would tend to increase the magnetoresistance with roughness.

The difficulty in making CPP measurements is due to the large surface area relative to the thickness of the samples. This results in a CPP resistance which is too small to measure using conventional techniques and also makes the measurements susceptible to inhomogeneous current paths. These difficulties have been overcome by making small area pillar samples,¹⁹ by using superconducting leads,²⁰ and by combinations of these two techniques.²¹ Experiments on Co/Ag multilayers find that the CPP magnetoresistance decreases with interface disorder while the CIP magnetoresistance increases.²² Cyrille *et al.* measured the CPP magnetoresistance of Fe/Cr multilayers and quantified the roughness in their samples using both low angle X-ray scattering and transmission electron micrographs of cross-sectional samples.^{21,23} They find that $\Delta\rho/AF$ increases with roughness proportionally to the RMS deviation in the layer heights. Still more recent experiments by Zambano *et al.* see no change in the CPP magnetoresistance of Fe/Cr multilayers with increasing roughness.²⁴

The effect of long length scale interface fluctuations is therefore unclear, with some work pointing to an increase in the magnetoresistance, some a decrease, and some no change at all. Some of the differences between the experiments is due to changing a growth parameter like the sputtering pressure probably changes more than just the interfacial roughness. A theoretical calculation can vary just the interface fluctuations and hence hope to isolate the effect of long length scale interface fluctuations on the magnetoresistance. While the earlier theoretical work is consistent with the CIP magnetoresistance experiments, the CPP magnetoresistance experiments remain unexplained. In particular the extensive work of Cyrille *et al.*^{21,23} which shows an increase in the magnetoresistance with interface roughness is not possible to explain as a mixing of the CPP and CIP geometries since the CIP magnetoresistance is usually lower than the CPP one, as is the case in their measurements.

In this paper we examine the effects of long length scale fluctuations in the layer thicknesses and heights using the

Boltzmann equation. A semiclassical approach like the Boltzmann equation is a good choice for this problem because the length scales involved are large compared to the atomic spacing. Various versions of the Boltzmann equation have also been used extensively in modeling the GMR.^{25,26,27,28} The Boltzmann equation we use here has a simple, but current conserving form for the scattering term, and we can solve it essentially exactly numerically in the limits of long and short mean free paths. Here, a long mean free path is much larger than the layer thicknesses, and a short mean free path is much smaller than the layer thicknesses. We consider both the CPP and CIP geometries and find that the GMR can either increase or decrease with interface roughness depending on the parameters in the problem. Explicit predictions are made for when the GMR increases and when it decreases.

The remainder of the paper is organized as follows. In Sect. II we provide a formal solution to the Boltzmann equation which is valid for arbitrary mean free paths. Next, in Sect. III we apply this formal solution to reproduce the well known results for the CIP and CPP geometries when the interfaces are flat. In Sect. IV we consider sinusoidal interfaces, which model the long length scale interface fluctuations. Both the long mean free path case (Sect. IV A) and the short mean free path case (Sect. IV B) are considered. These two cases are compared numerically in Sect. IV C. In Sect. V we use the results from Sect. IV to determine the effect of long length scale interface disorder on the giant magnetoresistance in the long mean free path case (Sect. V A) and the short mean free path case (Sect. V B). In Sect. V C the changes in the CPP and CIP resistivities due to increasing long length scale roughness are estimated in the long and short mean free path cases using experimentally determined parameters. All the results are summarized in the conclusion, Sect. VI.

II. FORMALISM

The model system we study is shown in Fig. 1. Multilayers of thickness Δy are separated by sinusoidal interfaces with amplitude A and period ξ . Within each layer the relaxation time, τ_i , is constant. For numerical considerations, our calculations are performed in two dimensions, namely the multilayers are strips in a two-dimensional plane; however, we nonetheless expect the results to remain qualitatively the same when generalized to three dimensions. Moreover, in both the long and short mean free path limits we will present analytic expressions for our results, which have direct generalizations to the three-dimensional case.

The Boltzmann equation we use represents elastic s-wave scattering within a current-conserving right-hand side,

$$\mathbf{v} \cdot \nabla_r f - e\mathbf{E} \cdot \nabla_p f = -\left(\frac{f - \bar{f}}{\tau}\right), \quad (1)$$

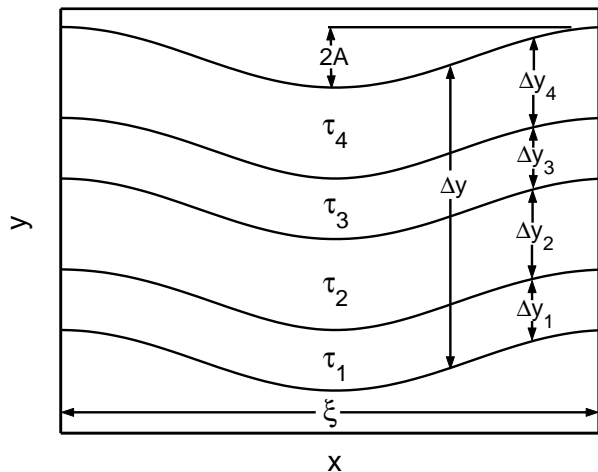


FIG. 1: Schematic of a four-layer repeat unit with interfacial roughness. The interfaces are modeled as sine waves of amplitude A and period ξ . Layer i has a thickness Δy_i and uniform relaxation time τ_i , and the total thickness of the repeat unit is Δy . We calculate the current density and conductivity due to roughness for currents flowing in the y -direction (CPP configuration) and x -direction (CIP configuration) for mean free paths which are long and short compared to Δy .

where $f = f(\mathbf{r}, \mathbf{p})$ is the distribution function, $\bar{f} = \bar{f}(\mathbf{r}, |\mathbf{p}|)$ is the spherical average of f in momentum space, and $\tau = \tau(\mathbf{r})$ is the relaxation time. To get the linear response conductivity the distribution function is expanded to first order in the applied electric field, $f = f_{eq} + \delta f$, where f_{eq} is the equilibrium Fermi-Dirac distribution function and δf is proportional to the applied electric field, \mathbf{E} . The linear response Boltzmann equation is

$$\mathbf{v} \cdot \nabla_r \delta f - e\mathbf{E} \cdot \mathbf{v} \left(\frac{\partial f_{eq}}{\partial \epsilon} \right) = - \left(\frac{\delta f - \bar{\delta f}}{\tau} \right). \quad (2)$$

This equation may be further simplified using the fact that the temperature is far below the Fermi temperature in these metals. Consequently, the energy derivative of the equilibrium Fermi function in Eq. (2) is approximately a delta function which pins the energy to the Fermi energy. One can define another distribution function on the Fermi surface, g ,

$$\delta f = \left(- \frac{\partial f_{eq}}{\partial \epsilon} \right) g \quad (3)$$

so that the Boltzmann equation becomes

$$\mathbf{v} \cdot \nabla_r g + e\mathbf{E} \cdot \mathbf{v} = - \left(\frac{g - \bar{g}}{\tau} \right). \quad (4)$$

This first order differential equation can be integrated to find g and hence f . As a first step the deviation of g from its spherical average \bar{g} is defined as δg ,

$$\delta g = g - \bar{g}. \quad (5)$$

Substituting δg into Eq. (4), the Boltzmann equation on the Fermi surface is now

$$\mathbf{v} \cdot \nabla_r \delta g + \frac{\delta g}{\tau} = -e\mathbf{E} \cdot \mathbf{v} - \mathbf{v} \cdot \nabla_r \bar{g}. \quad (6)$$

Both the gradient of the electrical potential, $\mathbf{E} = -\nabla\phi$, and the gradient of \bar{g} appear on the right hand side of Eq. (6). Consequently, it is useful to define the electro-chemical potential, V ,

$$V = \phi - \frac{\bar{g}}{e}, \quad (7)$$

so that there is only a single gradient on the right-hand side,

$$\mathbf{v} \cdot \nabla_r \delta g + \frac{\delta g}{\tau} = e\mathbf{v} \cdot \nabla V. \quad (8)$$

Equation (8) can be solved by integrating along paths in phase space. Letting $(\mathbf{r}(s), \mathbf{p}(s))$ be a trajectory in phase space which satisfies the equation of motion, $\dot{\mathbf{r}} = \mathbf{v}$ and $\dot{\mathbf{p}} = 0$, the distribution function along this path is

$$\tilde{g}(s) = \delta g(\mathbf{r}(s), \mathbf{p}(s)). \quad (9)$$

Substituting Eq. (9) into Eq. (8), one obtains a first order ordinary differential equation,

$$\frac{d\tilde{g}}{ds} + \frac{\tilde{g}}{\tau} = e \frac{dV}{ds}. \quad (10)$$

The general solution of this equation is

$$\begin{aligned} \tilde{g}(s_f) &= \exp \left(- \int_{s_i}^{s_f} \frac{1}{\tau(s)} ds \right) \tilde{g}(s_i) \\ &+ \int_{s_i}^{s_f} \exp \left(- \int_s^{s_f} \frac{1}{\tau(s')} ds' \right) e \frac{dV}{ds} ds, \end{aligned} \quad (11)$$

where s_i and s_f represent the initial and final coordinates in phase space, respectively. Note that with these simple equations of motion for this Boltzmann equation, the trajectories are lines, $\mathbf{p}(s) = \mathbf{p}_i = \mathbf{p}_f$ and

$$\mathbf{r}(s) = \mathbf{r}_f - \mathbf{v}(s_f - s). \quad (12)$$

When the starting point of integration is taken to infinity, $s_i \rightarrow -\infty$, Eq. (11) simplifies to

$$\tilde{g}(s_f) = \int_{-\infty}^{s_f} \exp \left(- \int_s^{s_f} \frac{1}{\tau(s')} ds' \right) e \frac{dV}{ds} ds. \quad (13)$$

Equation (13) is the starting point for the calculations in this paper. Solving it is not always straightforward because the electro-chemical potential is not known a priori. In some cases one can deduce V from general principles. In other cases Eq. (13) must be solved self-consistently as described below.

Once one has a solution to $\tilde{g} = \delta g(\mathbf{r}(s), \mathbf{p}(s))$, the current density, j , can be obtained directly from

$$j_\alpha(\mathbf{r}) = -eN(E_F) \int \frac{d\theta_p}{2\pi} v_\alpha \delta g(\mathbf{r}, \theta_p) \quad (14)$$

because \bar{g} has no angular dependence. In this equation the density of states at the Fermi surface is $N(E_F) = m/(\pi\hbar^2)$. For the nonuniform samples considered in this paper, the current density and the electric field will vary with position. An effective conductivity, σ , for the entire sample is defined using the spatial average of the current density, $\langle \mathbf{j} \rangle$, and the electric field, $\langle \mathbf{E} \rangle$,

$$\langle j_\alpha \rangle = \sigma_{\alpha,\beta} \langle E_\beta \rangle. \quad (15)$$

This is the conductivity one would obtain by measuring the net current and voltage drop for a large sample and multiplying by the usual factors of length and cross-sectional area. In Eq. (15) the conductivity is defined in terms of the electric field instead of the gradient of the electro-chemical potential. However, because of the periodicity in the multilayers, \bar{g} is periodic. Thus $\langle \nabla \bar{g} \rangle = 0$ because the spatial average of the derivative of a periodic function is zero. Consequently, from Eq. (7) the average electric field, $\langle \mathbf{E} \rangle$, is the same as the average gradient in the electro-chemical potential, $\langle -\nabla V \rangle$.

III. FLAT INTERFACES

In this section we apply the formalism developed in the previous section to solve the case of flat interfaces ($A = 0$ in Fig. 1). This will provide the basis for the calculations with wavy interfaces in the next section, since in this case we are able to solve the Boltzmann equation exactly for arbitrary mean free paths. It will also allow us to demonstrate that this formalism reproduces the conventional results in the limit of weak spin-flip scattering.

A. CPP geometry

In the Current-Perpendicular-to-Plane (CPP) geometry the current flows in the y -direction of Figure 1. Current conservation and translational symmetry in the x -direction imply that the current density is uniform throughout the sample. Translational symmetry also implies that the electro-chemical potential, V , only depends on the y variable. The actual functional form of $V(y)$, however, is not known a priori.

In order to determine $V(y)$ or equivalently dV/dy , the condition that the spherical average of δg is zero (see Eq. (5)) was used in conjunction with Eq. (13). This leads to an integral equation for dV/dy . Because of the periodicity of the multilayers and hence dV/dy , the infinite integral can be converted to a finite integral. Discretizing dV/dy then leads to a linear equation, which is easily solved numerically.

The results of this numerical calculation show that for all mean free paths the derivative of the electro-chemical potential in the i^{th} layer is proportional to the inverse of τ_i . Substituting this result into Eq. (13), it follows that the distribution function is independent of position

and proportional to $\hat{\mathbf{y}} \cdot \hat{\mathbf{p}}$, where $\hat{\mathbf{p}}$ is the direction of the momentum. The current is uniform as expected. Current uniformity and the fact that dV/dy within a layer is proportional to $1/\tau_i$ imply that the resistance is the same as one would obtain by adding classical resistors in series. The series resistor model for the CPP geometry is commonly used to analyze experiments in the limit of weak spin-flip scattering.²⁹

B. CIP Geometry

In the Current-in-Plane (CIP) geometry the current flows in the x -direction of Figure 1. In this case the electric field must be constant because of the symmetry of the problem and $\nabla \times \mathbf{E} = 0$. Furthermore, if we make the ansatz that $\bar{g} = 0$, then Eq. (13) can be integrated analytically. The spherical average of the resulting distribution function, δg , is indeed zero, which is consistent with the ansatz that $\bar{g} = 0$. Thus, in this case we also have a complete analytic solution for the distribution function.

Figure 2 shows the CIP current density in a two-layer repeat unit multilayer with $\Delta y_1 = 3$ and $\Delta y_2 = 7$. Each curve corresponds to different mean free paths, ranging from much less than to much greater than Δy . For comparison, the curves are normalized by the maximum of \mathbf{j}_x . As the figure illustrates, when the mean free paths are much less than Δy , \mathbf{j}_x changes rapidly at the interface. Moreover, in this limit the ratio of the current density in layer 2 to that in layer 1 equals the ratio of the corresponding mean free paths, which is what one would expect for classical macroscopic resistors in parallel. As the mean free paths increase, the current density smooths out, becoming roughly uniform across the repeat unit as the mean free paths become much greater than the layer thicknesses.

C. Summary

In the long mean free path limit the current density and the distribution functions in both geometries are independent of position. As seen in Eq. (13), there is an average over a mean free path which goes into computing the distribution function. If the mean free path is large enough, then the average effectively smears out the variations in the sample, producing a homogeneous current and distribution function.

In the short mean free path limit the current density is the same as one would obtain classically from adding resistors in series (CPP geometry) or in parallel (CIP geometry). In this case the integral used to calculate the distribution function, Eq. (13), is short ranged and in particular much smaller than the layer thicknesses. Each layer behaves like a macroscopic piece of metal.

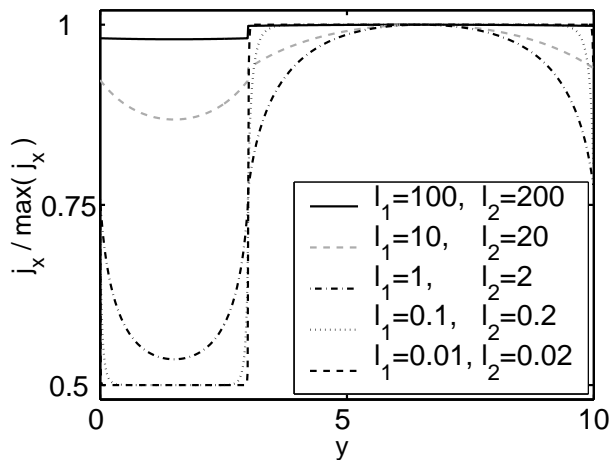


FIG. 2: CIP current density for different mean free paths in a two-layer repeat unit with $\Delta y_1 = 3$ and $\Delta y_2 = 7$. The mean free path in layer i is $l_i = v_F \tau_i$. For comparison, the current density \mathbf{j}_x for each curve is normalized by its maximum value, $\max(\mathbf{j}_x)$. In the short mean free path limit ($l_1, l_2 \ll \Delta y$) the current density changes sharply in proportion to l_1/l_2 across the boundary. Conversely, in the long mean free path limit ($l_1, l_2 \gg \Delta y$) the current density is roughly uniform.

IV. CURVED INTERFACES

For the case of the wavy interfaces shown in Fig. 1 it is not possible to obtain simple analytical expressions for the distribution function like the ones for the flat interface cases of the previous section. Moreover, direct numerical solution of the Boltzmann equation requires the solution of a three-dimensional problem (two space coordinates and one angular variable along the Fermi surface). However, we saw in the previous section that there are two natural limiting cases: (i) the long mean free path case, where the current density and distribution function are uniform, and (ii) the short mean free path case, where the current density and distribution function are determined by the local gradient in the electro-chemical potential. In this section we solve for the distribution function, current density, and conductivity in these two limiting cases.

A. Long mean free path limit

In the case where the mean free path is long compared to the layer thicknesses the integral used in computing the distribution function (Eq. 13) averages the gradient in the electro-chemical potential over a large region of the sample. If the mean free path is long enough, then the gradient in the electro-chemical potential may be approximated by its average value. The distribution function

then becomes

$$\tilde{g}(s_f) = -e\mathbf{v} \cdot \langle \mathbf{E} \rangle \tilde{g}'(s_f) \quad (16)$$

$$\tilde{g}'(s_f) = \int_{-\infty}^{s_f} \exp\left(-\int_s^{s_f} \frac{1}{\tau(s')} ds'\right) ds, \quad (17)$$

where the angular brackets denote a spatial average. As discussed in Sect. II, the average of the gradient in the electro-chemical potential, $\langle -\nabla V \rangle$, is equal to the average electric field, $\langle \mathbf{E} \rangle$, for a periodic system.

In the previous section, where we considered flat interfaces, we did not include interface scattering in the interest of simplifying the calculation. The scattering rates changed as electrons went from one material to another, but there was no additional scattering due to the interfaces. Here we include interface scattering since it is crucial for comparing to experiments. We model a simplified surface scattering as infinitesimal layers of a higher-resistivity material. Surface scattering is included on the right-hand side of the Boltzmann equation of Eq. (1) in addition to the bulk scattering term, $1/\tau_b$,

$$\frac{1}{\tau(\mathbf{r})} = \frac{1}{\tau_b(\mathbf{r})} + \Gamma \sum_i \int dl \delta^2(\mathbf{r} - \mathbf{R}_i(l)), \quad (18)$$

where the integration runs along the i^{th} interface, $\mathbf{R}_i(l)$ is the position of the i^{th} boundary, and Γ is a parameter characterizing the surface scattering rate. Letting ζ be the angle between the velocity, \mathbf{v} , and the unit vector normal to the boundary with the convention that $0 \leq \zeta \leq \pi/2$, the integral in Eq. (17) from slightly below ($s = t_-$) to slightly above ($s = t_+$) the interface is

$$\int_{t_-}^{t_+} \frac{1}{\tau(s)} ds = \frac{\Gamma}{v_F \cos(\zeta)}. \quad (19)$$

Physically, this means that the probability of an electron being scattered at an interface is lowest when its trajectory is perpendicular to the boundary ($\zeta = 0$) and larger when it crosses the boundary at an angle.

To test the approximation of Eqs. (16) and (17) we now evaluate the integral of Eq. (17) numerically. The resulting function, \tilde{g}' , should be independent of both angle and position. Figure 3 shows $\tilde{g}'(\theta)$ versus θ for a multilayer composed of two-layer repeat units with $\xi = 10$, $\Delta y_1 = \Delta y_2 = 2.5$, $l_1 = 1000$, $l_2 = 2000$, and $v_F/\Gamma = 500$. The dashed and solid lines represent this sample at $A = 0$ and $A = 1$, respectively. The statistical noise present in the latter curve near $\theta = 0$ and $\theta = \pi$ corresponds to electrons whose trajectories run nearly parallel to the x axis. Although these electrons intersect significantly fewer interfaces than those that travel along the y axis, the interfaces can nevertheless be much more effective in scattering them if they intersect a boundary nearly tangentially within a few mean free paths. Therefore \tilde{g}' is highly sensitive to small changes in θ near $\theta = 0$ and $\theta = \pi$. Despite the magnitude and frequency of the fluctuations in this region, the noise averages to the

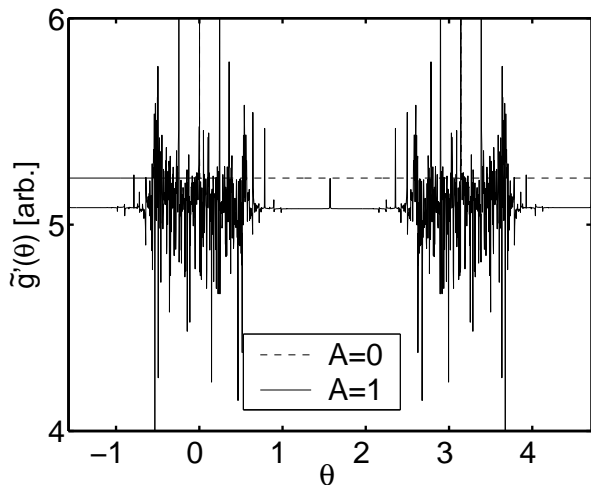


FIG. 3: The function $\tilde{g}'(\theta)$ used to compute the distribution function in the long mean free path limit. The fluctuations present near $\theta = 0$ and $\theta = \pi$ are due to paths which do not intersect many interfaces. Once these rapid oscillations are averaged locally, however, this function is roughly independent of angle and position as expected in the long mean free path limit. The decrease in \tilde{g}' as one goes from flat interfaces ($A = 0$) to curved interfaces ($A = 1$) leads to a decrease in the interface conductivity with roughness in both the CPP and CIP cases. The data shown correspond to a two-layer repeat unit with $\xi = 10$, $\Delta y_1 = \Delta y_2 = 2.5$, $\ell_1 = 1000$, $\ell_2 = 2000$, and $v_F/\Gamma = 500$.

smooth value of \tilde{g}' seen in the vicinity of $\theta = \pm\pi/2$. This kind of averaging is performed to compute the current, Eq. (14), and the conductivity, Eq. (15). Thus, once the small angle fluctuations are averaged the function \tilde{g}' is independent of angle. We have also verified that it is independent of position for a given sample.

From Fig. 3 it is apparent that \tilde{g}' decreases with increasing interface roughness (A), resulting in a decreasing conductivity in both the CIP and CPP geometries. Performing the same calculation except without surface scattering ($\Gamma = 0$), one finds that the two values for \tilde{g}' are the same. In other words, with only bulk scattering in our model interface roughness does not effect the conductivity. In the long mean free path limit, it is therefore necessary to have interface scattering in order to have a change in the conductivity with roughness.

In order to examine the additional contribution to the resistance due to interface scattering, we define an interface conductivity, σ^* , which is extracted as follows. For a given geometry the conductivities with and without interface scattering are computed, $\sigma_{\Gamma \neq 0}$ and $\sigma_{\Gamma = 0}$, respectively. Treating the bulk and interface resistances as resistors in series, the interface conductivity is given by

$$\sigma^* = \frac{M}{\Delta y} \left(\frac{1}{\sigma_{\Gamma \neq 0}} - \frac{1}{\sigma_{\Gamma = 0}} \right)^{-1}, \quad (20)$$

where M is the number of layers in a repeat unit and Δy

is the thickness of a repeat unit. In the example above the number of layers is $M = 2$ and the length of a repeat unit is $\Delta y_1 + \Delta y_2 = 5$. Using a resistors in series model is natural in the CPP geometry; however, it may be less clear that this is a good model for the CIP geometry. Here, because \tilde{g}' is independent of angle, the changes in the CPP and CIP conductivities are equal. Thus, what works in one geometry will also work in the other.

For a given set of bulk and surface scattering rates define $\delta\sigma^*$ as the difference between the interface conductivity for $A \neq 0$ and $A = 0$,

$$\delta\sigma^* = \sigma^*(A) - \sigma^*(0). \quad (21)$$

Figures 4 (a) and (b) contain plots of $|\delta\sigma^*/\sigma^*|$ versus $(A/\xi)^2$ for the CPP and CIP geometries, respectively. From Eq. (16) one can see that the distribution function $\delta g = \tilde{g}$ in the CIP case, where the average electric field is in the x -direction, is largest near $\theta = 0$ and $\theta = \pi$, while in the CPP case, δg is largest near $\theta = \pm\pi/2$. The larger scatter in the data of Fig. 4 for the CIP case than the CPP case reflects the larger scatter in \tilde{g}' near $\theta = 0$ and $\theta = \pi$.

The curves in these figures represent either various positions within a particular sample or fixed positions within samples that have different mean free paths or surface scattering rates. When plotted in this manner, all of the data fall onto the same line. Thus, not only is $\delta\sigma^*/\sigma^*$ proportional to $(A/\xi)^2$, but the proportionality constant is independent of the model parameters.

One difference between a curved interface and a flat interface is that the curved one is longer. Because of surface scattering, a curved interface will have more scattering and hence a larger resistance. The amount of extra scattering provided by a curved interface should be proportional to the additional length in the boundary. Let \mathcal{L} be the length of the interface and $\delta\mathcal{L}$ be the change in the interface length from the flat case ($A = 0$) to the wavy case ($A \neq 0$). The percent increase in the interface length, $\delta\mathcal{L}/\mathcal{L}$, is plotted as the \times 's in Fig. 4. To a good approximation it is evident from Fig. 4 that the percent decrease in the interface conductivity is equal to the percent increase in the length of the interface. For our sinusoidal boundaries the percentage change in the interface length is $\pi^2(A/\xi)^2$ for small A , so within our model we have

$$\frac{\delta\sigma^*}{\sigma^*} \approx -\frac{\delta\mathcal{L}}{\mathcal{L}} \approx -\pi^2 \left(\frac{A}{\xi} \right)^2. \quad (22)$$

B. Short mean free path limit

In the short mean free path limit the integral used to compute the distribution function, Eq. (13), samples the gradient in the electro-chemical potential over a short distance. Thus, we may approximate the electro-chemical

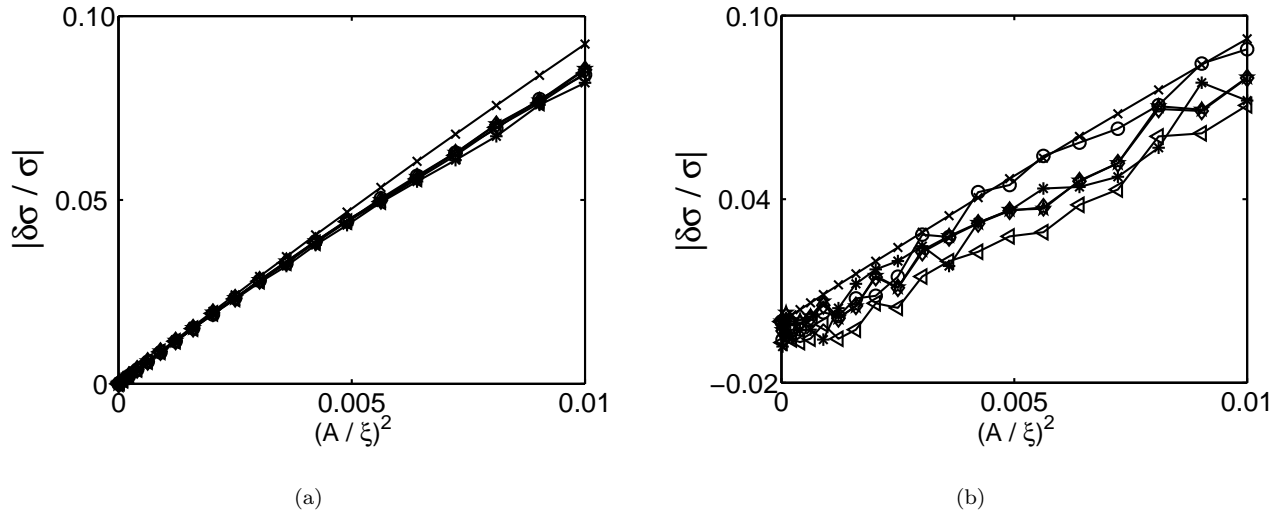


FIG. 4: Fractional change in the (a) CPP and (b) CIP interface conductivities with roughness in the long mean free path limit. Also shown is the corresponding change in interface length (\times) with roughness. In both cases the fractional change in the interface conductivity, $|\delta\sigma^*/\sigma^*|$, is very close to the fractional increase in the length of the interface, $\delta\mathcal{L}/\mathcal{L}$. In our model, which assumes sinusoidal interfaces, both of these quantities are proportional to $(A/\xi)^2$. The $(*)$, (o) , and (\diamond) data points represent different coordinates within a sample that has $\Delta y_1 = \Delta y_2 = 2.5$, $\ell_1 = 1000$, $\ell_2 = 2000$, and $v_F/\Gamma = 500$. The (\star) and (\triangleleft) points represent the same coordinate as the (\diamond) points, but correspond to samples with $\ell_1 = \ell_2 = 1000$ and twice the surface scattering rate, respectively. The larger scatter in the data for the CIP case is due to the fluctuations in \tilde{g}' in Fig. 3.

potential as constant within the integral, and the distribution function becomes

$$\delta g(\mathbf{r}, \hat{\mathbf{p}}) \approx e\tau v_F \hat{\mathbf{p}} \cdot \nabla V(\mathbf{r}). \quad (23)$$

In this approximation, the current density and conductivity in the i -th layer are given by

$$\mathbf{j}(\mathbf{r}) = \sigma(\mathbf{r})(-\nabla V(\mathbf{r})), \quad (24)$$

$$\sigma(\mathbf{r}) = \frac{ne^2\tau(\mathbf{r})}{m}. \quad (25)$$

Since the conductivity is constant within each layer, the current conservation condition, $\nabla \cdot \mathbf{j} = 0$, within a given layer implies that $-\nabla^2 V_i = 0$, where V_i is the electrochemical potential in layer i . The problem of finding the current density and effective conductivity due to roughness thus reduces to solving Laplace's equation within each layer subject to the boundary conditions that the current is conserved and that the electrochemical potential is continuous. As noted earlier, the average electric field, $\langle \mathbf{E} \rangle$, is the same as the average of the gradient in the electrochemical potential, $-\nabla V$, because of the periodicity of the multilayers.

Whereas in the long mean free path limit we had to include interface scattering or else there would not have been any effect, in the short mean free path limit there is already an effect without surface scattering. From calculations which include both bulk and surface scattering, we have found that the presence of interface scattering does not qualitatively alter the results for the conductivity. Thus, in the results presented below we do not include interface scattering.

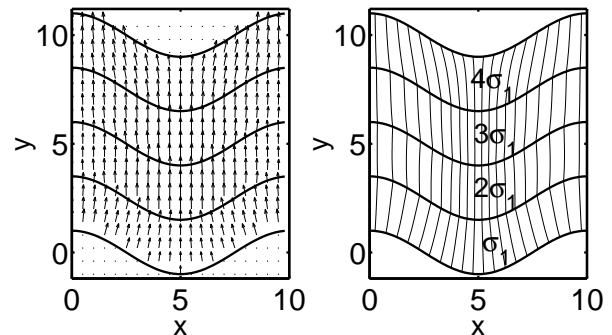


FIG. 5: CPP current density vector field and current field lines in the short mean free path limit. Due to roughness, current tends to traverse a greater distance in high conductivity than low conductivity layers, leading to an increase in the effective CPP conductivity with roughness.

Figure 5 shows the CPP current density vector field and current field lines in a repeat unit with $A = 1$, $\Delta y = \xi = 10$, $\Delta y_i = 2.5$, and $\sigma_i = i\sigma_1$. As the figure illustrates, roughness causes current to flow nonlinearly through the sample in such a way that it traverses a greater distance through the high conductivity layers than through the low conductivity layers. The effect of roughness is thus to increase the effective CPP conductivity, σ , of Eq. (15).

As in the long mean free path limit, the percentage increase in σ relative to the flat interface case is propor-

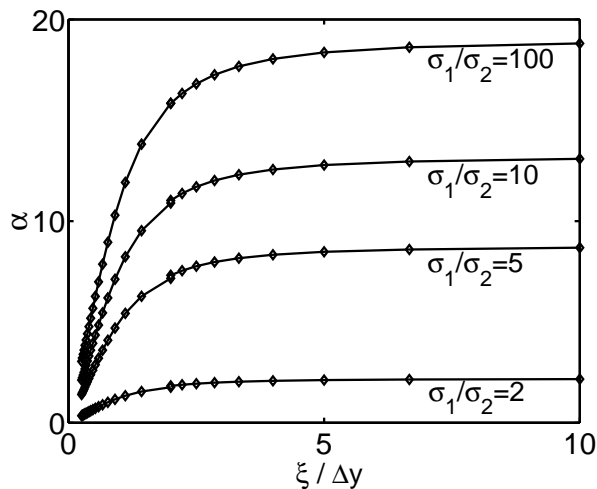


FIG. 6: The proportionality constant α_{CPP} between $\delta\sigma/\sigma$ and $(A/\xi)^2$ in the CPP geometry. This constant α_{CPP} increases with the ratio of the layer conductivities and $\xi/\Delta y$, saturating for $\sigma_1 \gg \sigma_2$ and when ξ becomes several times Δy .

tional to $(A/\xi)^2$,

$$\frac{\delta\sigma}{\sigma} \approx \alpha \left(\frac{A}{\xi} \right)^2. \quad (26)$$

Here, however, the proportionality constant, which we denote as α_{CPP} for the CPP case, depends on both the geometry and the layer conductivities. Figure 6 shows α_{CPP} as a function of $\xi/\Delta y$ for several values of σ_1/σ_2 for a sample composed of two-layer repeat units with $\Delta y_1 = \Delta y/2$. As the figure illustrates, α_{CPP} increases with the ratio of the layer conductivities and saturates for $\sigma_1 \gg \sigma_2$. It also increases with $\xi/\Delta y$, saturating as ξ becomes several times Δy .

To determine the current and conductivity in the CIP geometry, the same Laplace's equation is solved with the net potential drop in the x as opposed to the y direction. Figure 8 shows the CIP current density vector field and current field lines in a four-layer repeat unit with $A = 1$, $\Delta y = \xi = 10$, $\Delta y_i = 2.5$, and $\sigma_i = i\sigma_1$. Due to roughness, electrons in high conductivity layers impinge on lower conductivity layers near the interfaces. This in effect reduces the short circuit effect of the high conductivity layers and consequently decreases the effective CIP conductivity.

The percent change in the effective conductivity relative to the flat case ($A = 0$) is again proportional to $(A/\xi)^2$. The proportionality constant, α_{CIP} , is simply related to α_{CPP} in the two-layer case: α_{CIP} approximately equals the negative of α_{CPP} , where the latter is calculated with the layer conductivities interchanged ($\alpha_{CIP}(\sigma_1, \sigma_2) \approx -\alpha_{CPP}(\sigma_2, \sigma_1)$). Equivalently, α_{CIP} is roughly equal to the negative of α_{CPP} when the latter is computed for a sample in which the thicknesses of layers 1 and 2 are interchanged ($\alpha_{CIP}(\Delta y_1, \Delta y_2) \approx -\alpha_{CPP}(\Delta y_2, \Delta y_1)$). This result is illustrated in Fig.

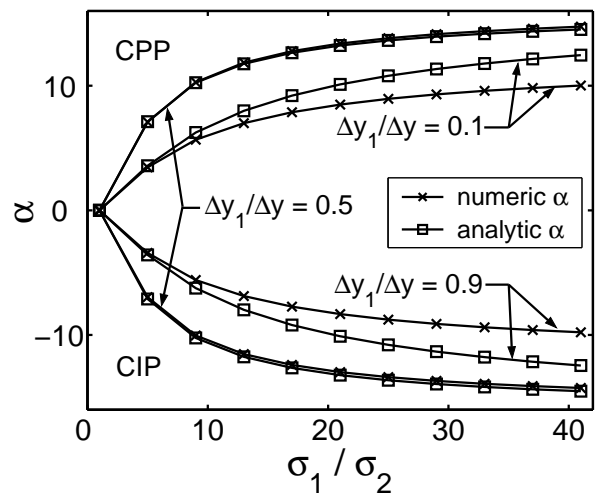


FIG. 7: Comparison of α for the CPP and CIP geometries. The numeric CPP and CIP curves shown are roughly mirror images of one another, illustrating that $\alpha_{CIP}(\sigma_1, \sigma_2) \approx -\alpha_{CPP}(\sigma_2, \sigma_1)$. Depending on the sample geometry, the analytical approximations for α in Eqs. (29) and (32) are excellent in some cases and only roughly correct in others. The data shown are for a two layer repeat unit with $\xi = 10$ and $\Delta y = 5.2$.

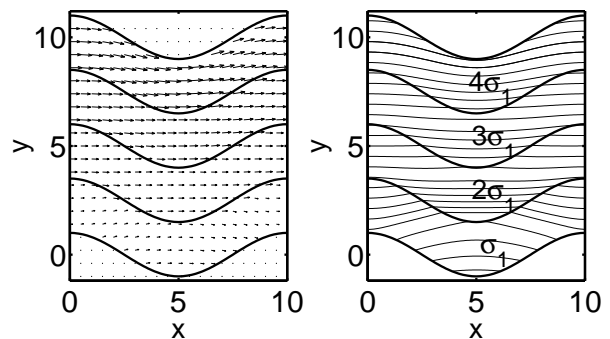


FIG. 8: CIP current density vector field and current field lines in the short mean free path limit. As a result of roughness, current near an interface does not remain within a single layer across a period but traverses both high and low conductivity regions. This reduces the short circuit effect of the high conductivity layers and leads to a decrease in the conductivity of the multilayer.

7, where the numeric α_{CPP} versus σ_1/σ_2 curves for $\Delta y_1/\Delta y = 0.5$ and 0.1 are mirror images of the numeric α_{CIP} versus σ_1/σ_2 curves for $\Delta y_1/\Delta y = 0.5$ and 0.9 .

Approximate analytic expressions for both α_{CIP} and α_{CPP} can be derived using the approach of Levy *et al.* for grooved multilayers¹⁶. These multilayers are similar to those shown in Fig. 1 except that the interfaces are piecewise linear. The angle the interfaces make with the x -axis is defined to be θ , and it is assumed that the layers are far apart relative to the amplitude of the interface fluctuations, which we have called A in the sinusoidal case. In the CIP configuration they approximate the electric field

to be uniform in the x -direction. Letting σ_{CIP} and σ_{CPP} be the CIP and CPP conductivities when the interfaces are flat, it follows that the spatial average of the current density is

$$\langle j_x \rangle = (\sigma_{CIP} \cos^2 \theta + \sigma_{CPP} \sin^2 \theta) E_x. \quad (27)$$

Consequently, the effective conductivity is

$$\sigma = \sigma_{CIP} \cos^2 \theta + \sigma_{CPP} \sin^2 \theta. \quad (28)$$

Although we consider sinusoidal as opposed to piecewise linear interfaces, we can use an approximate effective θ of $2A/(\xi/2) = 4A/\xi$. Expanding Eq. (28) for small θ and using the definition in Eq. (26), it follows that α in the CIP geometry is

$$\alpha_{CIP} \approx 16 \left(\frac{\sigma_{CPP}}{\sigma_{CIP}} - 1 \right). \quad (29)$$

Figure 7 shows α_{CIP} versus σ_1/σ_2 for different values of $\Delta y_1/\Delta y$ as computed analytically via Eq. (29) and numerically in the short mean free path limit. The data correspond to a sample composed of two-layer repeat units with $\xi = 10$ and $\Delta y = 5.2$. As the figure illustrates, the agreement between the analytic and numeric α_{CIP} is excellent for some parameters and worse for others. In the case of two-layer repeat units, we find the agreement to be particularly good when the geometric parameters satisfy $\xi/\Delta y_1 \approx 4$ for $\sigma_1 \geq \sigma_2$ and $\xi/\Delta y_2 \approx 4$ for $\sigma_1 \leq \sigma_2$. This relation is satisfied by the CIP curves corresponding to $\Delta y_1/\Delta y = 0.5$ in Fig. 7. In any case, the analytic expression does provide an estimate for α_{CIP} .

In the CPP case if one starts from Eq. (28) to obtain α_{CPP} , one obtains a poor fit to the numerical solution. In the CIP geometry for the case of flat interfaces, symmetry required that the electric field be uniform. On the other hand, in the CPP geometry for the case of flat interfaces, symmetry required that the current density be uniform. Thus, in the CPP geometry we start from the assumption that the current density is uniform in the y -direction. The average electric field in the y -direction is then

$$\langle E_y \rangle = (\rho_{CPP} \cos^2 \theta + \rho_{CIP} \sin^2 \theta) j_y, \quad (30)$$

where ρ_{CPP} and ρ_{CIP} are the CPP and CIP resistivities corresponding to flat interfaces. The effective resistivity is therefore

$$\rho = \rho_{CPP} \cos^2 \theta + \rho_{CIP} \sin^2 \theta \quad (31)$$

Note that this equation is not the same as Eq. (28) from Ref.¹⁶, but rather its generalization to the case of the CPP geometry. As will be shown below, it provides a much better fit to our numerical data on the CPP resistivity. Equation (31) and the assumption that $\theta \approx 4A/\xi$ imply that the CPP proportionality constant is the negative of the CIP proportionality constant,

$$\alpha_{CPP} = -\alpha_{CIP}, \quad (32)$$

independent of the sample geometry. Note, however, that numerically Eq. (32) holds for two-layer repeat units only when $\Delta y_1 = \Delta y_2$.

The analytic expression for α_{CPP} is compared to the numerical solution in Fig. 7. As for the CIP case, the analytic estimates are excellent for certain geometries but not as good for others. We find the agreement in the case of two-layer repeat units to be particularly good when the geometric parameters satisfy $\xi/\Delta y_2 \approx 3.7$ for $\sigma_1 \geq \sigma_2$ and $\xi/\Delta y_1 \approx 3.7$ for $\sigma_1 \leq \sigma_2$. The CPP curves corresponding to $\Delta y_1/\Delta y = 0.5$ in Fig. 7 satisfy this relation.

C. Comparison of the long and short mean free path limits

The physics of the change in the effective conductivity due to long length scale interface roughness is different in the long and short mean free path limits. The effect in the long mean free path limit is due entirely to enhanced interface scattering with roughness, and no effect is observed when surface scattering is ignored. In the short mean free path limit, interface scattering plays a less dominant role, as the effective conductivity changes with roughness even when only bulk scattering is present. Here the effect in the CPP geometry results from roughness providing a less-resistive, non-linear path of current flow, while the effect in the CIP geometry is due to a reduction of the short circuit effect of the high conductivity layers.

In the long mean free path limit, the decrease in the interface conductivity due to roughness approximately equals the corresponding increase in the interface length in both the CPP and CIP geometries. Thus, in our model we have

$$\frac{\delta\sigma^*}{\sigma^*} \approx -\frac{\delta\mathcal{L}}{\mathcal{L}} \approx -\pi^2 \left(\frac{A}{\xi} \right)^2. \quad (33)$$

In the short mean free path limit, the percent change in the effective conductivity due to roughness is also proportional to $(A/\xi)^2$,

$$\frac{\delta\sigma}{\sigma} \approx \alpha \left(\frac{A}{\xi} \right)^2. \quad (34)$$

Here, however, the proportionality constant α depends on the layer conductivities and the geometry of the sample. For a multilayer composed of two-layer repeat units with $\xi = 10$ and $\Delta y_1 = \Delta y_2 = 2$, the coefficient $|\alpha|$ is approximately 2 for $\sigma_1/\sigma_2 = 2$, 12 for $\sigma_1/\sigma_2 = 10$, and 18 for $\sigma_1 \gg \sigma_2$, indicating a range of order 10.

Within each limit, we make predictions concerning distinct physical quantities – interface conductivity versus effective conductivity. To compare the magnitude of the percentage change in the effective conductivity in both limits, we write $\delta\sigma/\sigma$ in the long mean free path limit in

terms of $\delta\sigma^*/\sigma^*$, where

$$\sigma = \left(\frac{1}{\sigma_{\Gamma=0}} + \frac{M}{\Delta y} \frac{1}{\sigma^*} \right)^{-1}. \quad (35)$$

Using Eq. (35) and the fact that $\sigma_{\Gamma=0}$ is independent of A , we find that

$$\frac{\delta\sigma}{\sigma} = \frac{\delta\sigma^*}{\sigma^*} \left(1 + \frac{\Delta y \sigma^*}{M \sigma_{\Gamma=0}} \right)^{-1}. \quad (36)$$

Since the second term in the parenthesis is greater than or equal to 0, $\delta\sigma/\sigma$ must be less than or equal to $\delta\sigma^*/\sigma^*$, where equality holds in the limit of zero bulk resistance. Additionally, $\delta\sigma/\sigma$ goes to zero in the absence of surface scattering. The constant of proportionality between $\delta\sigma/\sigma$ and $(A/\xi)^2$ therefore lies between 0 and $-\pi^2$ in the long mean free path limit. Comparing this range to the values of $|\alpha|$ stated above, we conclude that the magnitude of the percent change in the effective conductivity due to roughness can be greater in either the long or short mean free path limits.

V. GIANT MAGNETORESISTANCE

Magnetic multilayers are alternating layers of ferromagnetic and paramagnetic metals. For a large field in the plane of the layers, the magnetic moments of the ferromagnetic layers align, creating the parallel magnetic configuration (P). At zero or a lower field, the magnetic moments of the layers are not aligned in parallel. With a proper choice for the thickness of the paramagnetic layers, the ferromagnetic layers may be coupled antiferromagnetically so that adjacent magnetic layers have moments pointing in opposite directions. We call this the antiparallel (AP) configuration. The resistance of the multilayer in the two magnetic configurations is different, leading to a magnetoresistance. It is common to characterize this magnetoresistance as a ratio called the giant magnetoresistance or GMR,

$$GMR = \frac{\rho^{AP} - \rho^P}{\rho^P}, \quad (37)$$

where ρ^{AP} and ρ^P are the resistivities of the antiparallel and parallel configurations.

In many systems the spin relaxation length, which is how far an electron's spin maintains its orientation, is long compared to the thickness of the layers. Hence, it is often possible to approximate the resistance as being due to two parallel channels for conduction, one channel for each of the two possible spin orientations. In the following we make this approximation, the corrections to which are well known in both the CPP and CIP geometries^{26,30}.

A. Long Mean Free Path Limit

In order to deduce how the CPP GMR is effected by roughness in the long mean free path limit, within each

spin channel we treat the layers as resistors in series. First, let t_{PM} and t_{FM} be the thicknesses of the paramagnetic and ferromagnetic layers, respectively, and let $\Delta y = 2(t_{PM} + t_{FM})$. The resistivity for electrons of either spin in the paramagnetic material is denoted by ρ_{PM} , and the resistivity of the majority/minority electrons in the ferromagnetic material is $\rho_{FM,maj/min}$. The interface resistance for the majority/minority electrons is $\rho_{maj/min}^*$. Next, define ρ_{maj} and ρ_{min} by

$$\Delta y \rho_{maj} \equiv 2t_{PM}\rho_{PM} + 2t_{FM}\rho_{FM,maj} + 4\rho_{maj}^* \quad (38)$$

$$\Delta y \rho_{min} \equiv 2t_{PM}\rho_{PM} + 2t_{FM}\rho_{FM,min} + 4\rho_{min}^*. \quad (39)$$

In the parallel magnetic configuration, the resistivity of the majority spin channel is ρ_{maj} , and the resistivity of the minority spin channel is ρ_{min} . Adding the resistivity of the two spin channels in parallel gives a resistivity for the parallel configuration of

$$\rho_{CPP}^P = \frac{\rho_{min}\rho_{maj}}{\rho_{min} + \rho_{maj}}. \quad (40)$$

When the layers are aligned antiferromagnetically, both spin channels have the same resistivity, $(\rho_{maj} + \rho_{min})/2$. Adding the two spin channels in parallel gives an antiparallel configuration resistivity of

$$\rho_{CPP}^{AP} = \frac{1}{4}(\rho_{maj} + \rho_{min}). \quad (41)$$

As we have seen in the previous section, the effect of interface roughness in the long mean free path limit can be expressed as an increase in the interface resistance, $\delta\rho^*$. To determine the effect of interface roughness on the parallel resistivity, the antiparallel resistivity, and the GMR, we expand Eqs. (40), (41), and (37) to linear order in the changes in the interface resistances, $\delta\rho_{maj}^*$ and $\delta\rho_{min}^*$:

$$(t_{FM} + t_{PM})\delta\rho^P = \frac{2\rho_{min}^2}{(\rho_{maj} + \rho_{min})^2}\delta\rho_{maj}^* + \frac{2\rho_{maj}^2}{(\rho_{maj} + \rho_{min})^2}\delta\rho_{min}^* \quad (42)$$

$$(t_{FM} + t_{PM})\delta\rho^{AP} = \frac{1}{2}\delta\rho_{maj}^* + \frac{1}{2}\delta\rho_{min}^* \quad (43)$$

$$\delta GMR = \frac{1}{\Delta y} \left(\frac{1}{\rho_{maj}^2} - \frac{1}{\rho_{min}^2} \right) \times (\rho_{maj}\delta\rho_{min}^* - \rho_{min}\delta\rho_{maj}^*). \quad (44)$$

The changes in the interface resistances due to long length scale disorder may be obtained from Eq. (33) using the fact that ρ^* is the inverse of σ^* for both the majority and the minority electrons,

$$\frac{\delta\rho_{maj/min}^*}{\rho_{maj/min}^*} \approx -\frac{\delta\sigma_{maj/min}^*}{\sigma_{maj/min}^*} \approx \pi^2 \left(\frac{A}{\xi} \right)^2. \quad (45)$$

From Eq. (45) we can see that $\delta\rho^*$ is positive for both the minority and majority electrons. Consequently, in

the long mean free path limit both $\delta\rho^P$ and $\delta\rho^{AP}$ are positive, i.e., they increase with increasing long length scale interface disorder. On the other hand, the second term on the right hand side in Eq. (44) can be either positive or negative depending on the values of the resistivities and interface resistances. Hence when the electronic mean free paths are much greater than the layer thicknesses, the CPP GMR can either be enhanced or reduced by roughness depending on the sample. The same holds true for the CIP GMR since in the long mean free path limit the CPP and CIP resistances are the same.

B. Short mean free path limit

To compute the GMR in the short mean free path limit we consider a four-layer repeat unit with layers 1 and 3 being ferromagnetic and layers 2 and 4 being paramagnetic. As in the previous section, in the short mean free path limit we do not include interface scattering because it does not change the results qualitatively. Let $t_{FM} = \Delta y_1 = \Delta y_3$ be the thickness of the ferromagnetic layers and $t_{PM} = \Delta y_2 = \Delta y_4$ be the thickness of the paramagnetic layers. The conductivity for either spin direction in the paramagnetic layers is defined as σ_{PM} , and the conductivities for the majority and minority spins in the ferromagnetic material are $\sigma_{FM,maj}$ and $\sigma_{FM,min}$, respectively.

In the parallel magnetic configuration, the majority band electrons experience conductivities of $\sigma_1 = \sigma_3 = \sigma_{FM,maj}$ and $\sigma_2 = \sigma_4 = \sigma_{PM}$. Similarly, the minority band electrons experience conductivities of $\sigma_1 = \sigma_3 = \sigma_{FM,min}$ and $\sigma_2 = \sigma_4 = \sigma_{PM}$. When the magnetizations of adjacent ferromagnetic layers are aligned antiparallel, both spin channels have the same net conductivity since the ferromagnetic layers (1 and 3) have the same thicknesses and the paramagnetic layers (2 and 4) have the same thicknesses. The conductivity for either spin channel can thus be computed using $\sigma_1 = \sigma_{FM,maj}$, $\sigma_3 = \sigma_{FM,min}$, and $\sigma_2 = \sigma_4 = \sigma_{PM}$.

Solving Laplace's equation with the boundary conditions described in Sect. IV B, we compute numerically the conductivities for the parallel and antiparallel configurations, σ_P and σ_{AP} . The giant magnetoresistance then follows from Eq. (37), which when expressed in terms of the conductivity becomes $(\sigma_P - \sigma_{AP})/\sigma_{AP}$. In contrast to the CPP conductivity in either the parallel or antiparallel magnetic configurations, which always increases with long length scale interfacial roughness, we find that the CPP GMR can either increase or decrease with $(A/\xi)^2$ depending on the geometry of the sample and the layer conductivities. Specifically, for a sample with a given t_{FM} , t_{PM} , and $\sigma_{FM,maj/min}$, the GMR initially increases with roughness as σ_{PM} is increased from zero. At some point below $(\sigma_{FM,maj} + \sigma_{FM,min})/2$, σ_{PM} reaches a critical value at which the GMR is independent of roughness. The GMR subsequently decreases with roughness as σ_{PM} is increased beyond this value. This critical value, σ_{PM}^c ,

depends on the layer thicknesses and $\sigma_{FM,maj/min}$ and has the form

$$\sigma_{PM}^c = C(1 - \exp(-rt_{PM}/\Delta y)), \quad (46)$$

where C is a constant slightly below $(\sigma_{FM,maj} + \sigma_{FM,min})/2$ and r is a constant of order 10. The exact value of these constants depends on $\sigma_{FM,maj/min}$ and the layer thicknesses.

The CIP GMR in the short mean free path limit can be computed in the same manner as the CPP GMR by just changing the boundary condition from an applied field in the y -direction to an applied field in the x -direction. Here, we find the CIP GMR to be positive and proportional to $(A/\xi)^2$. In the short mean free path limit, the CIP GMR therefore vanishes only when the interfaces are flat ($A = 0$). Figure 9 shows the CIP GMR as a function of $\sigma_{PM}/\sigma_{FM,min}$ and $\sigma_{FM,maj}/\sigma_{FM,min}$ for a multilayer with $A = 1.5$, $\xi = 10$, $t_{FM} = 5.33$, and $t_{PM} = 2.67$. The CIP GMR increases as t_{PM} decreases, and within a particular geometry the GMR reaches its maximum value when $\sigma_{FM,maj} \gg \sigma_{FM,min}$ and $\sigma_{PM} \approx \frac{1}{2}\sigma_{FM,maj}$.

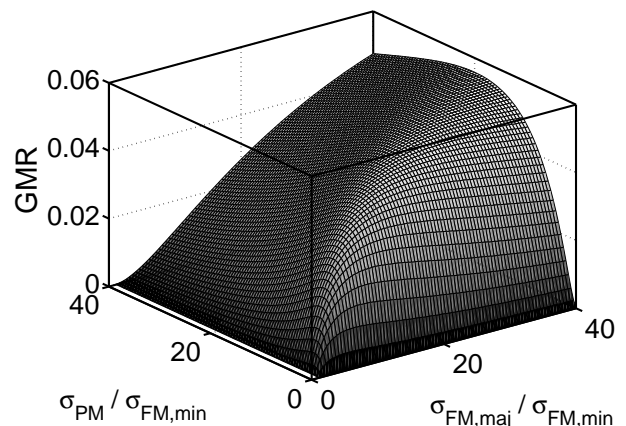


FIG. 9: Current-in-Plane GMR in the short mean free path limit. The presence of interfacial roughness leads to a giant magnetoresistance which is proportional to $(A/\xi)^2$ and thus vanishes only for $A = 0$. The conductivities of the paramagnetic layer (for either spin), the ferromagnetic majority bands, and the ferromagnetic minority bands are σ_{PM} , $\sigma_{FM,maj}$, and $\sigma_{FM,min}$, respectively. The maximum GMR is achieved when t_{PM} is small compared to t_{FM} and for $\sigma_{FM,maj} \gg \sigma_{FM,min}$ and $\sigma_{PM} \approx \frac{1}{2}\sigma_{FM,maj}$. The data shown correspond to a multilayer with $A = 1.5$, $\xi = 10$, $t_{FM} = 5.33$, and $t_{PM} = 2.67$.

In addition to solving for the conductivities exactly in the short mean free path limit, one can also use the approximate expressions of Eqs. (26), (29), and (32). Although not as accurate as the numerical solution, this technique may be useful in estimating the size of the effect for an actual experiment.

According to these equations the percent change in the conductivity due to long length scale surface roughness is proportional to the ratio of the CPP and CIP conductivities corresponding to flat interfaces. There are two

possible magnetic orientations of the layers, parallel and antiparallel. For each of these magnetic orientations the electrons can either be in the minority or majority bands. Thus, since there are two geometries (CPP or CIP), two magnetic orientations (P or AP), and two spin channels (maj or min), there is a total of eight conductivities to be specified. We denote the conductivity of the majority band for the CPP geometry in the parallel magnetic orientation as $\sigma_{CPP,maj}^P$ and label the other conductivities in a similar fashion.

For the CPP geometry the conductivities can be computed by adding the resistances of the layers in series. Using the notation for ρ_{maj} and ρ_{min} in Eqs. (38) and (39) with $\rho^* = 0$, the CPP conductivities are

$$\sigma_{CPP,maj}^P = 1/\rho_{maj} \quad (47)$$

$$\sigma_{CPP,min}^P = 1/\rho_{min} \quad (48)$$

$$\sigma_{CPP,maj}^{AP} = \sigma_{CPP,min}^{AP} = \frac{2}{\rho_{min} + \rho_{maj}}. \quad (49)$$

For the CIP geometry the conductivities can be computed by adding the resistances of the layers in parallel. It is useful to define the analog of Eqs. (38) and (39) for the layers in the parallel case,

$$\Delta y \sigma_{maj} \equiv 2t_{PM} \frac{1}{\rho_{PM}} + 2t_{FM} \frac{1}{\rho_{FM,maj}} \quad (50)$$

$$\Delta y \sigma_{min} \equiv 2t_{PM} \frac{1}{\rho_{PM}} + 2t_{FM} \frac{1}{\rho_{FM,min}}. \quad (51)$$

Note that with this notation $\rho_{maj} \neq 1/\sigma_{maj}$, which will be important below. The CIP conductivities are then

$$\sigma_{CIP,maj}^P = \sigma_{maj} \quad (52)$$

$$\sigma_{CIP,min}^P = \sigma_{min} \quad (53)$$

$$\sigma_{CIP,maj}^{AP} = \sigma_{CIP,min}^{AP} = \frac{\sigma_{min} + \sigma_{maj}}{2} = \frac{\sigma_{CIP}}{2}. \quad (54)$$

Within the two channel conduction model, for a given geometry and magnetic orientation the conductivity of the sample is the sum of the conductivities of the two spin channels. According to Eqs. (52) - (54), within this model the parallel and antiparallel configurations in the CIP geometry have the same sample conductivity, σ_{CIP} . Due to long length scale interface disorder each of the conductivities in Eqs. (47) - (54) changes according to Eqs. (26), (29), and (32). The net conductivity and resistivity of the sample therefore also change. As in the previous section we denote the change in the resistivity by $\delta\rho = -\delta\sigma/\sigma^2$. Here, the resistivities are different for the two geometries as well as the two magnetic orientations, so there are a total of four $\delta\rho$'s, which are given

below.

$$\delta\rho_{CPP}^P = 16 \left(\frac{A}{\xi}\right)^2 \left\{ \frac{\rho_{min}^2(\sigma_{maj}^{-1} - \rho_{maj})}{(\rho_{min} + \rho_{maj})^2} + \frac{\rho_{maj}^2(\sigma_{min}^{-1} - \rho_{min})}{(\rho_{min} + \rho_{maj})^2} \right\} \quad (55)$$

$$\delta\rho_{CPP}^{AP} = 16 \left(\frac{A}{\xi}\right)^2 \left\{ \frac{1}{\sigma_{CIP}} - \rho_{CPP}^{AP} \right\} \quad (56)$$

$$\delta\rho_{CIP}^P = 16 \left(\frac{A}{\xi}\right)^2 \frac{1}{(\sigma_{CIP})^2} \left\{ \sigma_{CIP} - \frac{1}{\rho_{CPP}^P} \right\} \quad (57)$$

$$\delta\rho_{CIP}^{AP} = 16 \left(\frac{A}{\xi}\right)^2 \frac{1}{(\sigma_{CIP})^2} \left\{ \sigma_{CIP} - \frac{1}{\rho_{CPP}^{AP}} \right\} \quad (58)$$

Using the definitions of ρ_{maj} , ρ_{min} , σ_{maj} , and σ_{min} , it follows that in the CPP geometry the change in resistivity is negative, $\delta\rho_{maj/min} < 0$, while in the CIP geometry the change in the resistivity is positive, $\delta\rho_{maj/min} > 0$. This result is expected from Figs. 5 and 8. In the CPP geometry the waviness of the interfaces allows the current to travel a greater distance through the less resistive layers, thereby reducing the resistance. In the CIP geometry the waviness of the interfaces disrupts the current flow through the low resistivity layers, increasing the resistance.

The GMR is determined by the ratio of the parallel and antiparallel resistivities. As seen above, the parallel and antiparallel resistivities either both increase or decrease depending on the geometry. Thus, one must compute their ratio explicitly to determine whether the GMR increases or decreases with long length scale interface disorder. Expanding Eq. (37) for the GMR to linear order in $\delta\rho_P$ and $\delta\rho_{AP}$ and substituting the changes in the resistivities of Eqs. (55) - (58), the change in the GMR for the CPP and CIP geometries is

$$\delta GMR_{CPP} = 16 \left(\frac{A}{\xi}\right)^2 \left\{ \left(\frac{1}{\sigma_{CIP}\rho_{maj}} - \frac{\rho_{CPP}^{AP}}{\sigma_{maj}\rho_{maj}^2} \right) + \left(\frac{1}{\sigma_{CIP}\rho_{min}} - \frac{\rho_{CPP}^{AP}}{\sigma_{min}\rho_{min}^2} \right) \right\} \quad (59)$$

$$\delta GMR_{CIP} = 16 \left(\frac{A}{\xi}\right)^2 \frac{1}{\sigma_{CIP}} \left\{ \frac{1}{\rho_{CPP}^P} - \frac{1}{\rho_{CPP}^{AP}} \right\}. \quad (60)$$

Using Eqs. (59) and (60), it can be shown that in the short mean free path limit the GMR decreases in the CPP geometry ($\delta GMR_{CPP} < 0$) and increases in the CIP geometry ($\delta GMR_{CIP} > 0$). In the CIP case, this result is consistent with our numerical computation of the GMR, which always increased with long length scale interface roughness. In the CPP case, however, we found numerically that the GMR could either increase or decrease with interface roughness depending on the sample geometry and the conductivities of the paramagnetic and ferromagnetic layers. In both geometries, Eqs. (59) and (60) generally yield much larger changes in the GMR than we predict numerically. This discrepancy is due to the fact

that the agreement between the analytic expressions for α and the numerical values varies depending on the layer conductivities. If the analytic and numeric values for α agree very well within a particular spin channel, then the analytic expression for the change in the conductivity for that channel will agree very well with the change computed numerically. When one considers a different spin channel with different layer conductivities, the analytic α will generally be a worse approximation of the numeric value because the layer conductivities have changed. The change in the conductivity for this channel computed analytically will likewise be a worse approximation of the numeric value. This will result in deviations between the antiparallel and parallel conductivities computed analytically and numerically. Since the GMR involves a ratio of these quantities, the error will be more significant in the GMR, resulting in large deviations between the analytic and numeric changes in the GMR.

C. Estimates

Both the long and short mean free path effects described in this paper must be present to some extent in any sample. The real question is how large these effects are and whether they can account for what is seen experimentally. In this section we estimate the size of the two effects in Fe(3nm)/Cr(1.2nm) multilayers using experimentally determined parameters. Although there are no adjustable parameters in these calculations, they are still merely estimates because the actual experiments are in neither the long nor the short mean free path limits, but somewhere in between. This can easily be seen from Cyrille *et al.*'s data²¹. In the long mean free path limit the CPP and CIP resistances are the same, whereas experimentally the ratio of the CPP to the CIP resistances is roughly 1.5. In the short mean free path limit there is no CIP GMR for flat interfaces, while there is roughly a 10% CIP GMR observed experimentally. In addition to taking the long and short mean free path limits, the calculations in this paper are performed in two dimensions instead of three dimensions, and we use one of the simpler Boltzmann equations.

To estimate the size of the long mean free path effect, we use Eqs. (42) and (43). The resistivities, ρ_{min} and ρ_{maj} , may be determined experimentally from Cyrille *et al.*'s measurements of ρ^P and ρ^{AP} using Eqs. (40) and (41). Although the data vary with the number of bilayers, the results depend only weakly on which data points one uses to compute ρ_{maj} and ρ_{min} , with the values in the range $\rho_{min} = 45.7 \pm 0.9 \mu\Omega cm$ and $\rho_{maj} = 130 \pm 8 \mu\Omega cm$. These are very close to the values obtained from Zambano's data³¹ of $\rho_{min} = 45 \mu\Omega cm$ and $\rho_{maj} = 143 \mu\Omega cm$, which is not surprising because the overall resistances in the two sets of experiments are close together, even though the trends are not the same.

To get the changes in the majority and minority surface resistances, $\delta\rho_{maj}^*$ and $\delta\rho_{min}^*$, one needs to know

the values of the surface resistances that the changes will be computed from. These parameters have not been determined in the experiments by Cyrille *et al.*; however, they have been determined in a series of experiments by Zambano *et al.* in which measurements were taken with different layer thicknesses and number of layers³¹. In their notation ρ_{maj}^* and ρ_{min}^* are equal to $AR_{Fe/Cr}^\uparrow$ and $AR_{Fe/Cr}^\downarrow$, respectively, and they find these values to be $\rho_{maj}^* = 2.7 f\Omega m^2$ and $\rho_{min}^* = 0.5 f\Omega m^2$. We will use these numbers for our estimate because the overall resistances in the two sets of experiments are close to one another.

Finally, we need to determine the waviness or roughness of the interfaces in the experiments. This was quantified by Cyrille *et al.* using two techniques – low angle x-ray diffraction and energy filtered imaging using cross-sectioned samples in a transmission electron microscope.²¹ Both techniques show that the root mean square deviation of the layer height increases within the multilayer and has the form $\sigma = \sigma_a M^\alpha$, where $\sigma_a = 0.37 nm$ is the root mean square deviation of the first bilayer, M is the bilayer index, and the exponent α equals 0.4. For the samples deposited at a constant pressure of 5mTorr, the average distance between surface bumps, or the period ξ in our model, was determined to be 10nm, independent of the bilayer index.²³ For a multilayer with N bilayers, the average value of $(A/\xi)^2$ used in Eq. (45) to compute the changes in the interface resistances is thus

$$\langle (A/\xi)^2 \rangle = \frac{1}{N} \sum_{M=1}^N (\sqrt{2}\sigma_a/\xi)^2 M^{2\alpha}, \quad (61)$$

where we have used the fact that the root mean square fluctuation for a sine wave is $A/\sqrt{2}$.

The result of using Eqs. (42), (43), (45), and (61) to estimate the size of the long mean free path effect is shown in Fig. 10. As expected both the parallel resistivity (solid line) and the antiparallel resistivity (dotted line) increase with roughness. The size of the increase in the antiparallel resistivity measured in the experiments by Cyrille *et al.* is comparable to this estimate for the antiparallel resistivity. However, our estimate of the size of the increase in the parallel resistivity is much larger than the negligible or possibly negative change in the parallel resistivity seen in the same experiments.

In the short mean free path limit, there are four resistivities for the two geometries (CIP and CPP) and magnetic configurations (P and AP). The changes in the resistivities for these four cases are given in Eqs. (55) - (58). In evaluating these equations, we use the CPP resistivities, ρ_{CPP}^P and ρ_{CPP}^{AP} , determined by the same ρ_{maj} and ρ_{min} used in the long mean free path limit using Eqs. (40) and (41). The CIP conductivity, σ_{CIP} , is taken to be in between the observed parallel and antiparallel conductivities: $(\sigma_{CIP})^{-1} = 25 \mu\Omega cm$. Finally, the conductivities σ_{maj} and σ_{min} are not readily determined from experiment. To estimate them, we impose the condition $\sigma_{maj}/\sigma_{min} = \rho_{min}/\rho_{maj}$ and use the value for

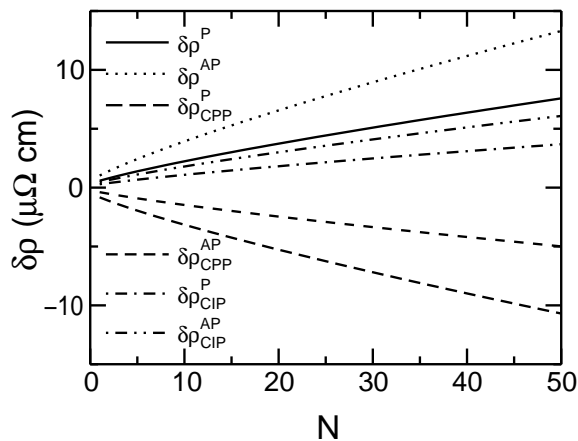


FIG. 10: Estimates in the long and short mean free path limits for the changes in the parallel and antiparallel resistivities due to long length scale interface roughness. The expressions for the changes in the resistivities are evaluated using experimentally determined parameters, but the data shown are only estimates because the experiments are in between the long and short mean free path limits. The magnitudes of the resistivity changes are consistent with those measured by Cyrille *et al.*; however, for intermediate mean free paths there can be cancellations of $\delta\rho^{P/AP}$ and $\delta\rho_{CPP}^{P/AP}$, which may explain the results of Zambano *et al.* For the CIP geometry there is no such cancellation and the estimates are comparable to the changes seen by Cyrille *et al.*

$\sigma_{CIP} = \sigma_{min} + \sigma_{maj}$ from above. The resulting changes in the resistivities are shown in Fig. 10. As expected, here the changes in the resistivities for the CPP configuration are negative, while the changes in the resistivities for the CIP configuration are positive. Although it was mentioned previously that the analytic expressions for the changes in the GMR given in Eqs. (59) and (60) predict a much larger effect in the short mean free path limit than we predicted numerically, the changes in the resistivities presented here are more reliable. Since the GMR involves a ratio of the antiparallel and parallel resistivities, the error in the analytic GMR will be more significant than the error in the analytic antiparallel and parallel resistivities.

As Fig. 10 illustrates, the changes in the CPP resistivities are of roughly the same magnitude, but opposite sign, in the long and short mean free path estimates. Thus, in a sample with intermediate mean free paths, there may be substantial cancellation of these two effects. For the CIP configuration, however, both the long and short mean free path effects tend to increase the resistivity by a similar magnitude. An increase in the CIP resistivity of comparable size to these estimates is indeed seen in the experiments by Cyrille *et al.*

These estimates show that the effects described in this paper are of the correct size to describe the observations of Cyrille *et al.*; however, detailed quantitative comparison is not possible because the mean free paths in the experiments are in between the long and short mean free

path limits. It is entirely possible that for intermediate mean free paths the two effects cancel, leading to the negligible change in the resistivity seen in the experiments by Zambano *et al.* If the long mean free path effect does dominate, then a result similar to that of Cyrille *et al.* would be observed. In the CIP configuration there are no complications due to the effects canceling. The estimated change in the resistivity in both limits is positive and comparable to the increase observed by Cyrille *et al.*

VI. CONCLUSIONS

In this paper we have examined the effect of interface disorder which is long on the atomic scale. These kinds of fluctuations are ubiquitous in metallic multilayers. A semiclassical Boltzmann equation was solved in both the limits where the electronic mean free paths were short and long compared to the layer thicknesses.

In the short mean free path case the current flow is nonuniform, and long length scale interface disorder increases the effective conductivity in the CPP geometry and decreases the effective conductivity in the CIP geometry. In the CPP case, the effect is due to interface disorder providing a less-resistive, non-linear path of current flow. In the CIP case, the effect results from interface roughness disrupting the flow of current through low resistance layers. In the long mean free path case the current flow is uniform in the CPP and CIP geometries. The resistance increases with long length scale interface roughness in both geometries because of the additional scattering created by longer interfaces for the disordered layers than the flat layers.

The experiments discussed in this paper are in neither the short nor the long mean free path limits, but somewhere in between. Nonetheless, in estimating the size of the long and short mean free path effects we find that in the CPP geometry the increase in the antiparallel resistivity observed by Cyrille *et al.* is comparable to the increase we predict in the long mean free path limit. The increase estimated in the CPP geometry for the parallel resistivity, however, is larger than the negligible increase measured by Cyrille *et al.* We find that the long and short mean free path effects tend to cancel for intermediate mean free paths in the CPP geometry, which could explain the observations of Zambano *et al.* For the CIP geometry, in both the long and short mean free path limits we estimate an increase in the resistivity that is comparable in magnitude to the increase seen by Cyrille *et al.* Therefore, the effects described here may be the source of the experimentally observed increase in the resistivity with long length scale disorder, although clearly more theoretical investigation is needed to understand the crossover between the long and short mean free path limits.

Acknowledgments

The authors would like to thank Tat-Sang Choy, Jack Bass, and Ivan Schuller for helpful discussions. This research was supported by DOD/AFOSR Grant No.

F49620-96-1-0026, the Center for Condensed Matter Sciences, the University Scholars Program at the University of Florida, and the National Science Foundation through the U.F. Physics REU Program.

-
- [†] Electronic address: alicej@physics.ucsb.edu
[‡] Electronic address: selman@phys.ufl.edu
- ¹ M. N. Baibich, J. M. Broto, A. Fert, F. Nguyen Van Dau, F. Petroff, P. Eitenne, G. Creuzet, A. Friederich, and J. Chazelas, *Phys. Rev. Lett.* **61**, 2472 (1988).
 - ² S. S. P. Parkin, N. More, and K. P. Roche, *Phys. Rev. Lett.* **64**, 2304 (1990).
 - ³ P. M. Levy, *Solid State Physics* **47**, 367 (1994).
 - ⁴ M. A. M. Gijs and G. E. W. Bauer, *Adv. Phys.* **46**, 285 (1997).
 - ⁵ J. Bass and W. P. Pratt, *J. Magn. Magn. Mater.* **200**, 274 (1999).
 - ⁶ A. Barthelemy, A. Fert, and F. Petroff, **12** (1999).
 - ⁷ M. Rühlig, R. Schäfer, A. Huber, R. Mosler, J. A. Wolf, S. Demokritov, and P. Grünberg, *Phys. Status Solidi A* **125**, 635 (1991).
 - ⁸ J. C. Slonczewski, *Phys. Rev. Lett.* **67**, 3172 (1991).
 - ⁹ E. E. Fullerton, D. M. Kelly, J. Guimpel, I. K. Schuller, and Y. Bruynseraede, *Phys. Rev. Lett.* **68**, 859 (1992).
 - ¹⁰ J. M. Colino, I. K. Schuller, V. Korenivski, and K. V. Rao, *Phys. Rev. B* **54**, 13030 (1996).
 - ¹¹ M. Velez and I. K. Schuller, *J. Mag. Magn. Mat.* **184**, 275 (1998).
 - ¹² R. Schad, J. Barnas, P. Beliën, G. Verbanck, C. D. Potter, H. Fischer, S. Lefebvre, M. Bessiere, V. V. Moshchalkov, and Y. Bruynseraede, *J. Magn. Magn. Matter* **156**, 339 (1996).
 - ¹³ R. Schad, P. Beliën, G. Verbanck, C. D. Potter, H. Fischer, S. Lefebvre, M. Bessiere, V. V. Moshchalkov, and Y. Bruynseraede, *Phys. Rev. B* **57**, 13692 (1998).
 - ¹⁴ R. Schad, P. Beliën, G. Verbanck, K. Temst, V. V. Moshchalkov, Y. Bruynseraede, D. Bahr, J. Falta, J. Dekoster, and G. Gangouche, *Europhys. Lett.* **44**, 379 (1998).
 - ¹⁵ J. Barnas and Y. Bruynseraede, *Phys. Rev. B* **53**, 5449 (1996).
 - ¹⁶ P. M. Levy, S. Zhang, T. Ono, and T. Shinjo, *Phys. Rev. B* **52**, 16049 (1995).
 - ¹⁷ T. Ono and T. Shinjo, *J. Phys. Soc. Jpn.* **64**, 363 (1995).
 - ¹⁸ M. A. M. Gijs, M. T. Johnson, A. Reinders, P. E. Huisman, R. J. M. van de Veerdonk, S. K. J. Lenczowski, and R. M. J. van Ganswinkel, *Appl. Phys. Lett.* **66**, 1839 (1995).
 - ¹⁹ M. A. M. Gijs, S. K. J. Lenczowski, and J. B. Giesbers, *Phys. Rev. Lett.* **70**, 3343 (1993).
 - ²⁰ S.-F. Lee, Q. Yang, P. Lolody, R. Loloee, J. H. Hetherington, S. Mahmood, B. Ikegami, K. Vigen, L. L. Henry, P. A. Schroeder, et al., *Phys. Rev. B* **52**, 15426 (1995).
 - ²¹ M. C. Cyrille, S. Kim, M. E. Gomez, J. Santamaria, K. M. Krishnan, and I. K. Schuller, *Phys. Rev. B* **62**, 3361 (2000).
 - ²² Wen-C. Chiang, W. P. Pratt, M. Herrold, and D. V. Baxter, *Phys. Rev. B* **58**, 5602 (1998).
 - ²³ J. Santamaria, M.-E. Gomez, M.-C. Cyrille, C. Leighton, K. M. Krishnan, and I. K. Schuller, *Phys. Rev. B* **65**, 12412 (2002).
 - ²⁴ Q. Yang, P. Holody, R. Loloee, L. L. Henry, W. P. Pratt, P. A. Schroeder, and J. Bass, *Phys. Rev. B* **51**, 3226 (1995).
 - ²⁵ R. E. Camley and J. Barnas, *Phys. Rev. Lett.* **63**, 664 (1989).
 - ²⁶ T. Valet and A. Fert, *Phys. Rev. B* **48**, 7099 (1993).
 - ²⁷ W. H. Butler, X.-G. Zhang, and J. M. MacLaren, *J. Appl. Phys.* **87**, 5173 (2000).
 - ²⁸ M. D. Stiles and D. R. Penn, *Phys. Rev. B* **61**, 3200 (2000).
 - ²⁹ S.-F. Lee, W. P. Pratt, Q. Yang, P. Holody, R. Loloee, P. A. Schroeder, and J. Bass, *J. Magn. Magn. Mater.* **118**, L1 (1993).
 - ³⁰ J. Chen and S. Hershfield, *Phys. Rev. B* **57**, 1097 (1998).
 - ³¹ A. Zambano, K. Eid, R. Loloee, W. P. Pratt, and J. Bass, *J. Magn. Magn. Mater.* in press (2002).